Local lattice distortion in $Si_{1-x-y}Ge_xC_y$ epitaxial layers from x-ray absorption fine structure

D. De Salvador,* M. Tormen,† M. Berti, and A. V. Drigo
Istituto Nazionale Fisica della Materia and Dipartimento di Fisica ''G.Galilei,'' University of Padova, Via Marzolo 8, I-35131 Padova, Italy

F. Romanato
Istituto Nazionale Fisica della Materia, Tecnologie Avanzate Superficie Catalisi, Laboratory at Elettra Synchrotron Strada Statale.14 Km 163.5 I-32 Basovizza, Trieste, Italy

F. Boscherini
Istituto Nazionale Fisica della Materia and Dipartimento di Fisica, University of Bologna, Viale C. Berti Pichat 6/2, 40127 Bologna, Italy

J. Stangl, S. Zerlauth, and G. Bauer
Institut für Halbleiterphysik, Johannes Kepler Universität Linz, Altenbergerstrasse 69, A-4040 Linz, Austria

L. Colombo
Istituto Nazionale Fisica della Materia and Dipartimento di Fisica, University of Cagliari, Cittadella Universitara, I-09042 Monserrato, Cagliari, Italy

S. Mobilio
Istituto Nazionale Fisica Nucleare, Laboratori Nazionali di Frascati, P.O. Box 13, I-00044 Frascati, Italy and Dipartimento di Fisica, University of Roma Tre, Via della Vasca Navale 84, 00146 Roma, Italy
(Received 23 August 2000; published 9 January 2001)

The local structure around Ge in an epitaxial film of $Si_{1-x-y}Ge_xC_y$ alloy is investigated by x-ray absorption fine structure. The interatomic distances and the Debye-Waller factors were determined as a function of the carbon concentration up to the third coordination shell. The most important effect of the introduction of C in the $Si_{1-x}Ge_x$ matrix is the increase of static disorder with C concentration. This effect is larger for higher coordination shells. Molecular dynamics simulations show that this effect is due to the strong deformations induced by the small C atoms in the $Si_{1-x}Ge_x$ matrix. The variation of interatomic distances as a function of C concentration and of the epitaxial strain is also discussed.

DOI: 10.1103/PhysRevB.63.045314 PACS number(s): 61.66.Dk, 61.10.Ht, 61.82.Fk, 61.43.Bn

I. INTRODUCTION

In recent years the physical properties and device applications of $Si/Si_{1-x}Ge_x$ heterostructures have been extensively studied. Recently, the introduction of carbon into the binary alloy has opened additional possibilities in the field of Si based heterostructures. Carbon allows the opportunities for tailoring the lattice constant[1] and the band gap[2] to be increased. Devices based on $Si_{1-x-y}Ge_xC_y$ heterostructures, such as a heterobipolar transistor with a $Si_{1-x-y}Ge_xC_y$ base region, have been suggested and realized (see Refs. 3 and 4 for a review).

Yet, some structural properties of the $Si_{1-x-y}Ge_xC_y$ alloy have not been fully investigated. In particular, while it is well established that even small amounts of carbon induce strong reductions in the *average* lattice parameter[1] (for a review, see, e.g., Ref. 5 and references therein), only a few experimental studies on the *local* effect of carbon in the lattice structure exist. In Refs. 6 and 7 Raman scattering was used as a local probe in order to investigate $Si_{1-x-y}Ge_xC_y$ and $Si_{1-y}C_y$ alloys, respectively. In these papers the experimental results are compared to the theoretical ones obtained from a valence force field model.[8] In particular, Ref. 7 indicates a preferential third-nearest-neighbor C-C ordering in $Si_{1-y}C_y$ alloys, as later confirmed by Simon *et al.*[9] using x-ray photoelectron diffraction. On the other hand, no direct experimental evaluation of the local interatomic distances and their distribution in $Si_{1-x-y}Ge_xC_y$ alloys is available to our knowledge.

One of the most direct experimental techniques that can be used to investigate the local atomic structure is the analysis of x-ray absorption fine structure (XAFS) spectra. Recent XAFS experiments succeeded in describing the local structure of $Si_{1-x}Ge_x$ alloys up to the first coordination shell.[10–13] Furthermore, XAFS reliability for studying the local effects of epitaxial strain on the first coordination shell[14–18] and the local environment up to the third shell[19,20] was demonstrated.

The local structure can be investigated also by theoretical methods such as molecular dynamics (MD) or Monte Carlo (MC) simulations. Particularly interesting for this specific material are the results obtained by using the Tersoff empirical potential for multicomponent systems.[21] Many structural aspects of $Si_{1-x-y}Ge_xC_y$ alloys were explained by MC simulations by Kelires (see Ref. 22 and references therein); in particular, the dependence of the lattice parameter on the composition quantitatively reproduces experimental results on $Si_{1-y}C_y$ (Ref. 23) and $Si_{1-x-y}Ge_xC_y$ alloys.[1] A recent-

MD work using the same potential shows quite good agreement with *ab initio* calculations for amorphous $Si_{1-y}C_y$.[24]

In this paper we report the results of an XAFS study at the Ge *K* edge on a series of pseudomorphic samples with constant Ge concentration (about 14 at. %) and an increasing content of C from 0 to 1.7 at. %. We demonstrate that small amounts of C deeply affect the XAFS signal, and show that this change can be explained by an increase of the local disorder introduced by C. A quantitative analysis of the disorder (i.e., the Debye-Waller factors) as well as of the interatomic distances is made up to the third coordination shell. The variation of the interatomic distances as a function of the C concentration and of strain is presented.

In order to understand how the C atoms can cause distortion of the $Si_{1-x}Ge_x$ matrix and to predict the interatomic distances, MD simulations were performed using the Tersoff potential.

In Sec. II the experimental and theoretical tools are described. In Sec. III the experimental and theoretical results for the interatomic distances and the Debye-Waller factors are reported. In the Discussion (Sec. IV) the theoretical and experimental results are compared. In particular, some theoretical atomic configurations causing strong deformation of the Ge-Si(Ge) distances are discussed.

II. METHODS

A. Growth and characterization

The samples were grown by molecular beam epitaxy using *e*-beam evaporators for Si, Ge, and C. The overall growth rate was typically 1 Å s^{-1}. All samples were grown on (001) oriented Si substrates, which were RCA cleaned *ex situ* and underwent oxide removal at 900°C in UHV. After the deposition of a Si buffer layer while the temperature was ramped down from approximately 600 °C to the alloy growth temperature, the $Si_{1-x-y}Ge_xC_y$ alloy layers were grown. A series of samples were grown with a nominal Ge concentration of 14 at. % while the C content varied from 0 to 2 at. %. The layer thickness was nominally 100 nm. Additionally, a $Si_{1-x}Ge_x$ sample of 2 μm thickness with a Ge content of 2 at. % (without carbon) was grown as a measurement standard.

Conventional Rutherford backscattering spectrometry (RBS), carried out with a 2 MeV $^4He^+$ ion beam delivered by the AN2000 accelerator facility at the Laboratori Nazionali di Legnaro, provided the determination of the Ge fraction and layer thickness.[25] The RBS spectra were analyzed by fitting the experimental data with numerically calculated spectra, considering appropriate geometrical factors and stopping power functions.[26,27] The overall typical error on the Ge concentration measured with this procedure is about ± 0.4 at. %. No information about the C content can be gained from these RBS spectra, mainly because of the very low value of the Rutherford cross section for this element and the low C content of the samples.

High resolution x-ray diffraction (HRXRD) ω-2θ scans around the (004) Bragg reflection were measured using a Philips MRD diffractometer equipped with a four-crystal Ge (220) Bartels-type monochromator. From these scans the lattice parameters in the growth direction $a_\perp$ were determined. From reciprocal space maps around (004) and (224) Bragg reflections, the in-plane lattice parameter $a_\parallel$ was obtained, and from $a_\perp$ and $a_\parallel$ the corresponding relaxed lattice parameters a_0 were calculated. The results of RBS and HRXRD structural characterization are summarized in Table I. As described in Sec. III A, the C concentration was obtained by combining RBS and HRXRD data.

TABLE I. Main results of the XRD and RBS characterization.

Sample	*x* (at. %) (± 0.4)	$a_\perp$ (Å)	a_0 (Å)	*y* (at. %) (± 0.1)	$\epsilon_\parallel$ %
A	13.5	5.478	5.458	0.00	-0.49
B	12.6	5.453	5.443	0.52	-0.23
C	13.9	5.428	5.429	1.20	0.03
D	14.8	5.418	5.423	1.51	0.14
E	14.1	5.406	5.417	1.73	0.26
F	1.8	5.436	5.434	0.00	-0.06

B. XAFS measurements and data analysis

XAFS measurements at the Ge *K* edge were performed at the European Synchrotron Radiation Facility (ESRF) in Grenoble (France) at the GILDA beam line, using a dynamically sagitally focusing Si(311) monochromator;[19] higher order harmonics were rejected by a pair of grazing incidence, Pd coated mirrors. The measurements were performed in the 10 900–12 200 eV energy range; samples were kept at 77 K in order to reduce the thermal damping of the signal. The spot size was approximately 1×2 mm^2 and the photon flux approximately 5×10^{10} photons per second. Fluorescence detection was performed with a seven-elements hyperpure Ge detector. Particular care was taken in order to have a linear response in the fluorescence signal: the shaping time of the amplifiers was 0.25 μs and the total count rate on each detector element was limited to 30 000 counts/s. Furthermore, all the samples from *A* to *E* have a quite similar Ge concentration profile thus producing the same average count rate and the same residual nonlinearity effects. The integration time was chosen in order to keep the statistical error smaller than 1.5 parts per thousand. Comparison of the seven signals from the multidetector allows us to recognize detector saturation due to Bragg reflections that reach one or more of the detectors directly. This spurious effect was eliminated by excluding the saturated channels in calculating the average of the seven independent signals. Another possible artifact is the modulation of the fluorescence intensity due the excitation of x-ray standing waves occurring in a narrow energy range. This second spurious effect was eliminated by using a vibrating sample holder.[18] In order to detect possible structural anisotropies due to the strain induced by epitaxial growth,[28] each spectrum was collected twice using different sample orientations with respect to the polarization of the x rays: the polarization was chosen to be either nearly parallel ($\parallel$) to the film surface (75° between the polarization direc-

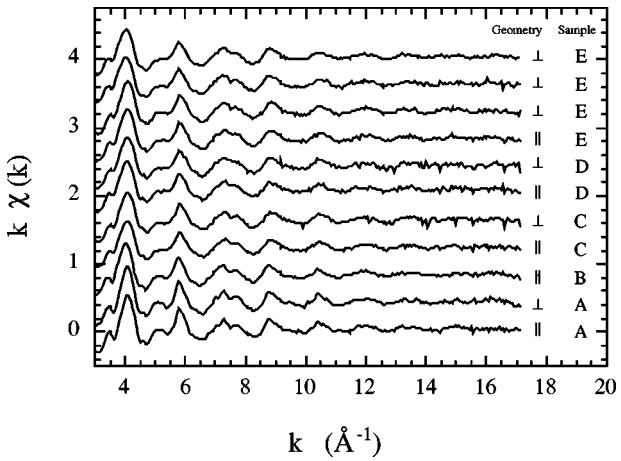

FIG. 1. Raw XAFS signals. The symbols ∥ and ⊥ are referred to the orientation of the photon beam polarization with respect to the interface plane. Capital letters refer to the different samples (see Table I).

tion and the surface normal), or nearly perpendicular (⊥) to the surface (20° between the polarization direction and the surface normal).

XAFS oscillations were extracted from the raw data using the AUTOBK code.[29] The preedge region was fitted with a linear function while the atomic background was estimated with a cubic spline. The extracted XAFS oscillations plotted versus the photoelectron wave vector k are shown in Fig. 1.

Data analysis was performed by an *ab initio* modeling of the XAFS signal.[30] The theoretical signals were calculated by means of a model cluster containing Si and Ge atoms in an undistorted diamond structure with a lattice parameter equal to that of Si. The Si and Ge atoms were distributed in the cluster in order to generate all the possible single and multiple scattering signals up to the third shell. A cluster with a C atom in every shell was also generated in order to estimate the contribution of C to the signals. Analysis of the signals of this trial cluster led us to the conclusion that the Ge-C signals can be completely neglected due to the low C content of the sample and the weak scattering amplitude of the C atoms.

Both the theoretical and experimental data $\chi(k)$ were multiplied by a weighting function k^w and Fourier transformed in the k range $[k_{min},k_{max}]$ before performing the fitting of the experimental spectra. The FEFFIT program[31] was used to extract structural parameters. For all the coordination shells the experimental signal was fitted with a linear combination of Ge-Ge and Ge-Si contributions. The total coordination number (N) of each shell was kept constant at the value in the diamond structure, i.e,. $N=4$ for the first shell and $N=12$ for the second and third shells. The relative weight of the Ge-Si and Ge-Ge signals was fixed on the basis of the average Ge concentration obtained by RBS assuming a random arrangement of the Ge and Si atoms. The fitting parameters for the first shell were $r_{1st}^{Ge\text{-}Si}$, the Ge-Si bond length, $r_{1st}^{Ge\text{-}Ge}$, the Ge-Ge bond length, and a common value of the Debye-Waller factor (σ_{1st}); for the second and third shells the fitting parameters were: r_{2nd} (a common distance for the Ge-Si and Ge-Ge second shells), r_{3rd} (for the Ge-Si and Ge-Ge third shells), and their Debye-Waller factors (σ_{2nd} and σ_{3rd}, respectively). For all shells nonstructural fitting parameters were the many-body amplitude reduction factor S_0^2 and the threshold energy E_0. A single distance was used for the second shell although it is well known that different combinations of Si and Ge give rise to unequal interatomic distances.[32] The motivations for this choice are a reduction in the number of free fitting parameters and our interest in the modifications induced by the presence of C. However, it has been found that this is an excellent approximation given the relatively low Ge concentration and the magnitude of the Debye-Waller (DW) factor. The fit was performed in two steps: in the first we optimized the first shell parameters, and in the second step the second and third shell parameters were optimized while keeping constant the values of the first shell interatomic distances and Debye-Waller factors. For this structure the first shell signals extend to higher k values than the second and third shell signals. For this reason different values of w and k_{max} were used while fitting the first and the higher shells. The first fitting step was performed in the R-space interval [1.4,2.7] Å on data filtered using $w=2$ and $k_{max}=14$ Å^{-1} ($k_{min}=3.8$ Å^{-1}). In the second step the fit was performed in the R interval [1.4,4.5] Å on data filtered using $w=1$ and $k_{max}=11.5$ Å^{-1} ($k_{min}=3.8$ Å^{-1}).

The most important multiple scattering (MS) signals due to triangular atomic arrangements were also included in the fits. However, MS signals are almost negligible in the k region of the fits and become important only at lower k values.

C. Theoretical methods

The Tersoff potential described in Ref. 21 is a many-body potential developed in order to investigate multicomponent systems containing Si, C and Ge atoms. The potential is an extension of the single component potential[33] obtained by introducing a single new parameter for each pair of atomic species. These parameters are taken from Ref. 21 for the Si-Ge and Si-C and from Ref. 22 for the Ge-C pair.

MD simulations were carried out by a fifth order predictor corrector algorithm applied to a periodically repeated cubic cell containing $N=1000$ atoms distributed in a diamond lattice. The adopted time step is as small as 0.5 fs for an optimal integration of the equations of motion. Two different statistical ensembles were used in the simulations. The first is the standard constant-temperature, constant-pressure (N-P-T) ensemble in which the temperature is controlled by velocity rescaling and the volume changes are governed by Andersen's equations.[34,35] The second ensemble adopted here consists in a slight modification of the N-P-T ensemble. We have essentially kept the volume constant along the x and y lateral dimensions, while keeping the pressure constant only along the z direction. This ensemble will be referred to as the N-P_z-T ensemble and was controlled by means of a minor modification of the Andersen method which in this case is used to properly reproduce the epitaxial strain typical of the samples investigated.

The starting configurations were obtained with the atoms randomly distributed in the sites of a perfect diamond structure. In the case of the N-P-T ensemble, the starting lattice parameter is obtained from Ref. 1 according to the Ge and C composition of the sample. When the N-P_z-T ensemble is used, a_x and a_y are fixed to the silicon values in order to simulate a pseudomorphic epitaxial constraint while the starting a_z value is calculated on the basis of elasticity theory. In both cases a simulated annealing procedure was followed to relax internal strain, and final equilibration as well as direct calculation of relevant properties were performed at 77 K and vanishing external pressure to reproduce the experimental conditions. The typical simulation strategy was actually through 5×10^4 steps used to equilibrate the samples (i.e., to allow for damping of temperature and pressure oscillations) followed by 2×10^4 steps during which the correlation functions were averaged. Some trial simulations with longer equilibration times or a higher temperature equilibration were made as well: the correlation functions obtained were in rather close agreement with those obtained with the standard procedure. Five C compositions from 0 to 2 at. % were studied, while the Ge content was kept constant at 14 at. %. For each composition ten configurations were created to perform an accurate configurational average of the system. Typical variations of some 10^{-3} Å in the lattice parameters and in the average interatomic distances were observed for different starting configurations.

III. RESULTS

A. Experimental results

Table I reports the results of the HRXRD and RBS sample characterization. The Ge concentration x of samples A to E varies in the range from 12.6 to 14.8 at. % with a mean value of 13.8 at. %. The variation is due to small fluctuations in the growth conditions. Sample F has a composition of 1.8 at. %. The HRXRD and RBS measurements confirmed the nominal value of the layer thickness, 100 nm for samples A-E, and 2000 nm for sample F.

The HRXRD measurements confirmed that all epilayers are grown pseudomorphically onto the Si substrates. The experimental values of $a_\perp$, $a_\parallel$, and x can be used in order to determine the C concentration y, using the Poisson effect and the dependence of the relaxed alloy lattice parameter a_0 from the Ge and C compositions reported in Ref. 1.

In Fig. 2 we report the Fourier transform (continuous line) of a spectrum of sample $A(y=0)$ and the average (bars) of three Fourier transforms of three independent spectra of sample E (highest C content $y=1.73$ at. %). These three spectra were collected at the beginning, in the middle, and at the end of the measurement run and systematically exhibit a lower amplitude with respect to all the other collected spectra. A simple inspection of the plot shows that carbon induces a significant change in the local structure of the alloy: it is evident that C induces a reduction in all the shell signals, the effect being more pronounced the higher the shell distance.

The fits shown in Fig. 3 demonstrate that all the features of the experimental signals are well reproduced by the theory. The interatomic distances obtained for all the samples from A to E are reported in Fig. 4 as a function of the C concentration. In the lower panel the first shell Ge-Si (squares) and Ge-Ge (triangles) bond lengths are reported. The other panels report the average second and third shell distances. Open and closed symbols are relative to signals taken with the beam polarization almost parallel and perpendicular to the layer-substrate interface, respectively. The statistical errors on the distance value are ±0.005 Å for the Si-Ge first shell distance, ±0.02 Å for the Ge-Ge first shell, ±0.01 Å for the second shell, and ±0.02 Å for the third shell. The bond lengths are almost constant within the error bars while the second and third shells slightly decrease. No significant changes in the interatomic distance as a function of the polarization direction are detected.

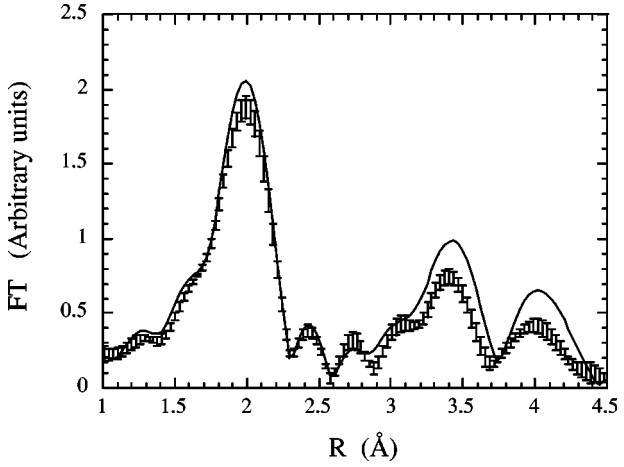

FIG. 2. Fourier transform (FT) of signal of sample A in $\perp$ geometry (continuous line) and average Fourier transform of three spectra of sample E in $\perp$ geometry (bars). The amplitude of the bars indicates the scattering of the data of the three spectra.

Figure 5 reports the Debye-Waller factors of all the shells as a function of the C concentration. It appears that the DW factors continuously increase with the C content and that this

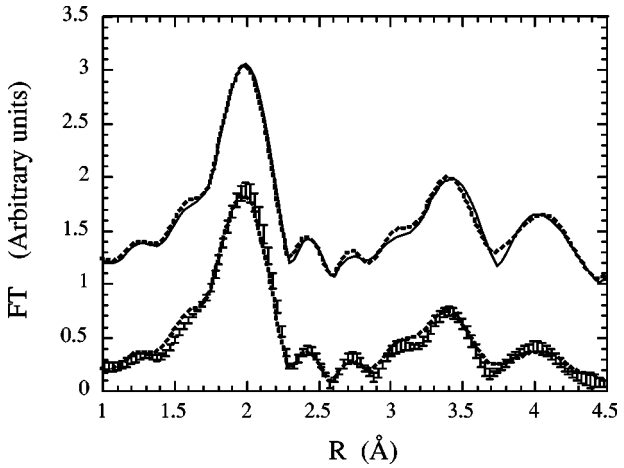

FIG. 3. The experimental Fourier transforms of Fig. 2 (continuous line and bars) are redrawn together with their fits (dotted lines). The data of sample A are shifted upward by one unit.

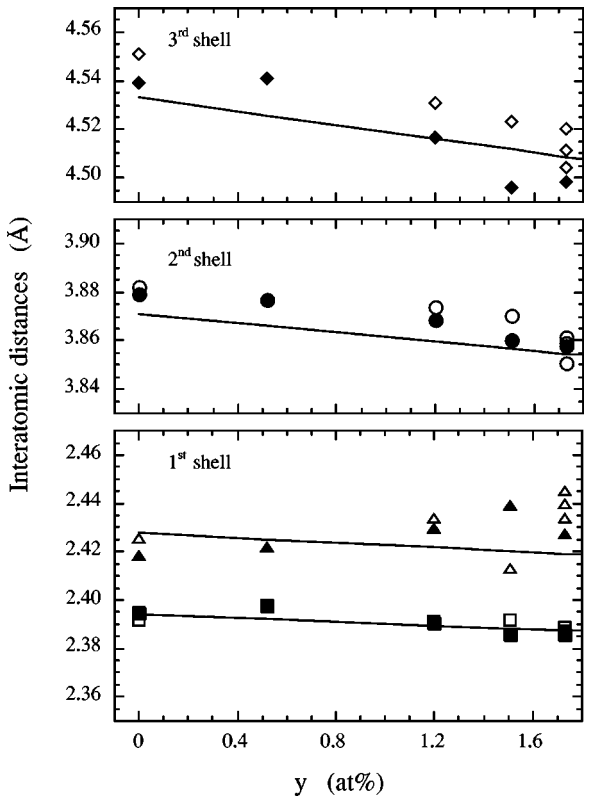

FIG. 4. Plot of the interatomic distances for the three coordination shells. First shell: squares, Ge-Si; triangles, Ge-Ge; second shell: circles; third shell: diamonds. Closed symbols are relative to the ∥ geometry, open symbols correspond to the ⊥ geometry. The continuous lines are linear fits of the theoretical results.

effect is more pronounced for the higher shells. From a linear fit of the data we can deduce that 1 at. % of carbon induces an increase in the DW factors of about $(0.7\pm0.3)\times10^{-2}$ Å, $(1.5\pm0.3)\times10^{-2}$ Å, and $(2.1\pm0.3)\times10^{-2}$ Å for the first, second, and third shells, respectively (see Table II).

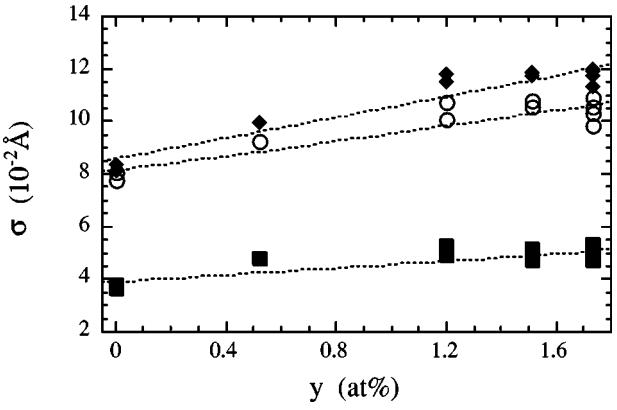

FIG. 5. Debye-Waller factors of the three coordination shells. First shell, squares; second shell, circles; third shell, diamonds. The dashed lines are linear fits to the data.

TABLE II. DW factor increase for 1 at. % of carbon.

Shell	Experimental increase (10^{-2} Å) (±0.3)	Theoretical increase (10^{-2} Å)
1	0.7	0.3
2	1.5	1.0
3	2.1	1.4

B. Theoretical results

The theoretical calculations allow us to determine the partial particle-particle correlation functions around the Ge atoms which can be directly compared to the XAFS results. In other words, we calculate the probability function $G_{\text{Ge-}A}(r)$ of finding a given atomic species A at a distance r from a Ge atom. As an example, the upper panel of Fig. 6 shows the sum of the partial correlation functions $G_{\text{Ge-Si}}(r)$ and $G_{\text{Ge-Ge}}(r)$ [hereafter simply referred to as $G(r)$]. The continuous line corresponds to a $Si_{0.84}Ge_{0.14}C_{0.02}$ alloy while the dashed line is relative to $Si_{0.86}Ge_{0.14}$.

Gaussian fits of the calculated shell peaks allow us to obtain information about the shell distances and their broadening. In Fig. 4 the results of four sets of interatomic distances are reported as a function of the C composition (continuous lines) for a direct comparison to the experimental data. Two sets of distances are relative to the first shell and are obtained from the $G_{\text{Ge-Si}}(r)$ and $G_{\text{Ge-Ge}}(r)$ partial correlation functions. The second and third shell distances were obtained from the sum of the Ge-Si and Ge-Ge correlation

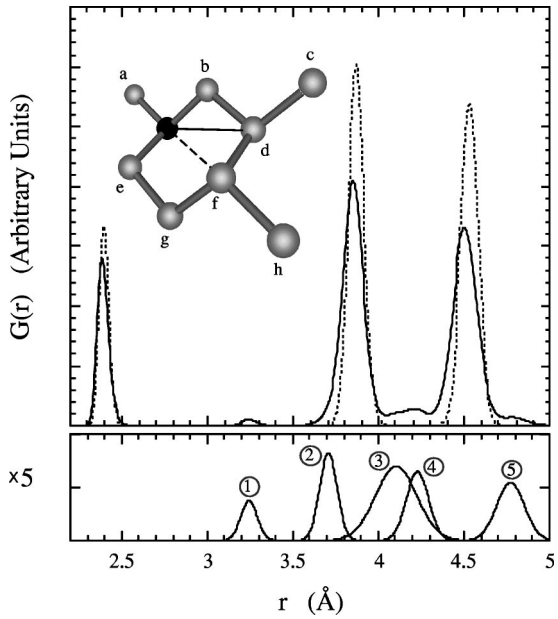

FIG. 6. Theoretical calculations of the radial correlation function $G(r)$. In the top panel the dashed line is relative to 14 at. % Ge and C, while the continuous line is relative to the same amount of Ge and 2 at. % C. The bottom panel shows the five minor peaks of the 2 at. % C correlation function; the y axis is magnified by a factor of 5. The inset in the top panel represents a cluster of atoms surrounding the absorber (black atom).

functions. This procedure allows coherent comparison of second and third shell theoretical results with the experimental data, which are obtained assuming a single value for the Ge-Si and Ge-Ge interatomic distances. The MD simulations based on the *N-P-T* ensemble show that the introduction of C in the $Si_{1-x}Ge_x$ alloy induces a reduction in the interatomic distances. This decrease for the second and third shells is more pronounced than for the first shell. The theoretical prediction (full line) of the trend for the interatomic distances versus C content in the alloy is in rather good agreement with the reported experimental data.

IV. DISCUSSION

The experimental data show the following local effects due to the introduction of C in a $Si_{1-x}Ge_x$ matrix: (i) the bond lengths are almost constant inside the error bars; (ii) the second and third shell distances decrease with increasing C concentration; (iii) the Debye-Waller factors increase more obviously the greater the interatomic distance.

The experimental interatomic distances are quite well reproduced by the theoretical data in the *N-P-T* ensemble, i.e., without taking into account any external strain effect. In other words, the alloying effect (i.e., the variation of the interatomic distances with the composition due to the accommodation of internal strain) is sufficient to properly describe the interatomic distance trend. On the other hand, Refs. 17, 18, 20, and 36 demonstrated that epitaxial external strain can induce a deformation in the interatomic distances which can be added to the alloying deformation. In particular, all the first shell distances decrease (increase) under compressive (tensile) strain while the second and third shells are split into two subsets of interatomic distances when the unit cell is tetragonally distorted. The first subset, with the interatomic distances almost parallel to the growth direction, has the same qualitative behavior as the first shell distances, whereas the second subset, with interatomic distances almost perpendicular to the growth direction, undergoes deformations of opposite sign.[20]

MD calculations performed taking into account the epitaxial constraint confirm this general trend. When no C is present in the alloy, the layer is under compressive strain. In this case the theoretical calculations predict a decrease of about 0.004 Å in the first shell distances. In contrast, the tensile strain induced by addition of 2 at. % of C increases the interatomic distance by about 0.003 Å. Thus the strain effect on the first shell compensates the bond length decrease induced by the alloying, and the predicted bond lengths are constant as a function of the C concentration at values of about 2.389 Å and 2.422 Å for Ge-Si and Ge-Ge bonds, respectively. These values are quite consistent with the experimental data.

As far as the second and third shell distances are concerned, the theoretical data predict the presence of splittings due to the strain effects. The difference between the interatomic distances of the two second shell subsets is about -0.021 Å for the $Si_{0.86}Ge_{0.14}$ layer, and 0.014 Å for $Si_{0.84}Ge_{0.14}C_{0.02}$. For the third shell the split values are -0.035 Å and 0.023 Å for $Si_{0.86}Ge_{0.14}$ and $Si_{0.84}Ge_{0.14}C_{0.02}$, respectively. Polarization dependent XAFS measurements in principle are sensitive to these effects since the contribution to the total XAFS signal of the differently oriented interatomic distances (subsets) changes according to the polarization direction. According to Ref. 20, the measurements performed with the two polarization directions should reproduce the splittings reduced by a numerical factor due to the fact that no complete separation between the two signals of the two subshells can be obtained experimentally. The predicted reduction of the splittings is 2.45 and 1.69 for the second and third shells, respectively. In this way the biggest split experimentally observed should be -0.009 Å and -0.021 Å for the second and third shells in the case of a $Si_{1-x}Ge_x$ alloy. These values are comparable to the measurement errors and hence no strain effect can be clearly established in our experiment (note that the strain values reported in Refs. 17, 18 and 20 were up to 0.02, i.e., four times larger than in our samples).

However, significant variations in the local alloy structure are detected both experimentally and theoretically due to the introduction of C (Fig. 2 and Fig. 6). As can be seen in Fig. 6 the most important change occurring when the C content is increased involves the *peak intensities* of the correlation function rather than a change in the shell interatomic *distances*. As a matter of fact the shell peaks undergo a strong broadening, leading to a peak intensity reduction; furthermore, new minor peaks appear. Five minor peaks with Gaussian shape can be identified; they are plotted separately in the bottom panel of Fig. 6 with a magnification factor equal to 5. These peaks correspond to strong deformations of the second or third shell distances due to particular atomic configurations involving a C atom. In order to describe these configurations, a cluster of atoms surrounding the absorber (black atom) is drawn in the inset of Fig. 6. In this inset two interatomic distances corresponding to the second and third shells are shown with a continuous and a dashed line, respectively, while every atom is marked by a letter. The atoms $(a,\text{absorber},b,c,d)$ and (e,f,g,h) lie in two parallel $(1\bar{1}0)$ planes and are joined by the absorber-*e* and *d*-*f* bonds along the $[1\bar{1}\bar{1}]$ direction. The atoms represented are the minimum set of atoms that allows all the kinds of atomic configuration generating the minor peaks to be shown. All the other atoms that complete the tetrahedral structures are omitted for simplicity.

The second or third distances evidenced in the figure undergo strong deformations according to the positioning of C atoms in particular sites of the cluster. In Table III the C site position generating each of the minor peaks is reported, together with its corresponding shell number (second or third). The relative intensity of the peaks (i.e., the fraction of the total coordination number due to the specific minor peak) is also reported in the table as a function of the C composition *y*. This value is obtained under the hypothesis of a random distribution of the atoms, since, the starting atomic configuration of the simulations are randomly sorted. It is demonstrated that ordering effects are in principle important in order to correctly describe C containing alloys. Indeed, a chemical repulsion between C and Ge was observed by MC

TABLE III. Minor peak properties. C position generating the peak (see inset of Fig. 6), coordination shell, and relative intensity as a function of C concentration are reported for each of the minor peaks.

Peak	C position	Shell	Abundance
1	*b*	2	*y*
2	*g*	2	2*y*
3	*c*,*a*	2	2*y*
4	*b*,*d*,*e*,*g*	3	4*y*
5	*a*,*h*	3	2*y*

calculations in Ref. 22, i.e., in our range of composition, Ge-C first neighbor bonds are less probable than in a random distribution. Such a behavior would reduce the intensity of some of the minor peaks. In particular, peak 1 would be reduced because it strictly depends on the presence of Ge-C nearest-neighbor (NN) bonds, peak 2 would be unchanged since it is caused exclusively by next-nearest-neighbor (NNN) Ge-C pairs, and the peaks from 3 to 5 would be reduced since half of the configurations generating them are related to NN Ge-C bonds.

In more detail, the peak number 1 is generated by an atomic configuration in which a C atom is at *b*, i.e., the C atom is a first neighbor of the absorber atom, bridging it to the second neighbor atom at site *d*. The shortening of the bond lengths *b*-absorber and *b*-*d* causes a strong reduction of the second shell distance. Peak 2 corresponds to a distance slightly smaller than the main second shell peak and it can be considered as the left hand tail of such peak. It is generated by second shell distances with a C atom at site *g*. This carbon atom attracts the absorber and its NNN at *d* causing them to get closer together. Peak 3 corresponds to an increase of the second shell distances due to a C atom at site *c* or *b*. The C atom at *c* attracts *d*, while the C atom at *a* attracts the absorber. In both cases the absorber-*d* distance increases. Peak 4 corresponds to a reduction of the third shell distance due to the presence of a C atom at one of the sites joining the absorber to the third shell atoms at *f*. Such a C atom reduces the path between the absorber and the *f* atom and therefore reduces the third shell distance. Peak 5 corresponds to a third shell distortion generated by the same mechanism as peak 3 with C atoms at *a* or *h*.

The presence of these minor peaks leads to a shape of the second and the third shell correlation functions quite different from the Gaussian shape imposed by the fit of the experimental data, and therefore makes it difficult to compare experimental and theoretical data. Furthermore, due to the experimental noise not all the details are reproduced or can be found in the experimental curves. The only way to compare the experimental and theoretical data is therefore to fit the theoretical $G(r)$ with the same fitting function used for the experimental data, i.e., Gaussian peaks with fixed total coordination number and Ge concentration. In this way we have extracted the DW theoretical variation as a function of the C concentration reported in Table II for the three coordination shells. Even if the theoretical DW factor increase is smaller than that of the experimental data, the general behavior is well simulated by the theoretical calculations.

V. CONCLUSION

In this work a detailed study of the local atomic environment around a Ge atom in a $Si_{1-x-y}Ge_xC_y$ alloy as a function of the C content was performed up to the third coordination shell. The XAFS experimental data show a decrease of the interatomic distance in the second and third shell, as a function of the C content, while the first shell Ge-Ge and Ge-Si distances are almost constant. MD calculations confirm that first shell distances are nearly constant and show that this is due to two competitive effects: the reduction due to C alloying and the increase due to the epitaxial strain variation. The second and third shell data are quite well reproduced by the theoretical calculation without taking into account the strain effect.

A strong reduction of the shell peak intensity is detected by increasing the C content. Such behavior is more evident for the farthest shells. The reduction of the peak shell intensity was fitted by a progressive increase of the Debye-Waller factor. Detailed MD simulations confirm the observed trend of an increase of the disorder with the shell distance. In particular, we found configurations leading to strong distortions of the second and third shell distances.

ACKNOWLEDGMENTS

The authors wish to thank F. Schäffler and L. Brambilla for useful discussions. XAFS measurements were performed at ESRF partially within the Public User Program. This work was partially supported by the EC program for Human Potential–Research Training Network, SIGENET Contract No. HPRN-CT-2000-00123.

*Electronic address: desalvador@padova.infm.it

†Present address: Physikalisches Institut, Universität Würzburg, Am Hubland, 97074 Würzburg, Germany.

[1] D. De Salvador, M. Petrovich, M. Berti, F. Romanato, E. Napolitani, A. Drigo, J. Stangl, S. Zerlauth, M. Mühlberger, F. Schäffler, G. Bauer, and P. C. Kelires, Phys. Rev. B **61**, 13 005 (2000).

[2] O.G. Schmidt and K. Eberl, Phys. Rev. Lett. **80**, 3396 (1998).

[3] K. Eberl, K. Brunner, and O.G. Schmidt, in *Germanium Silicon, Physics and Materials*, Vol. 56 of *Semiconductors and Semimetals*, edited by R. Hull and J.C. Bean (Academic Press, San Diego, 1999).

[4] S.C. Jain, *Germanium-Silicon Strained Layers and Heterostructures* (Academic Press, Boston, 1994).

[5] S.C. Jain, H.J. Osten, B. Dietrich, and H. Rücker, Semicond. Sci. Technol. **10**, 1289 (1995).

[6] B. Dietrich, H.J. Osten, H. Rücker, M. Methfessel, and P. Zaumseil, Phys. Rev. B **49**, 17 185 (1994).

[7] H. Rücker, M. Methfessel, B. Dietrich, K. Pressel, and H.J. Osten, Phys. Rev. B **53**, 1302 (1996).

[8] H. Rücker and M. Methfessel, Phys. Rev. B **52**, 11 059 (1995).
[9] L. Simon, L. Kubler, J. Groenen, and J.L. Balladore, Phys. Rev. B **56**, 9947 (1997).
[10] J.C. Woicik, K.E. Miyano, C.A. King, R.W. Johnson, J.G. Pellegrino, T.L. Lee, and Z.H. Lu, Phys. Rev. B **57**, 14 592 (1998).
[11] D.B. Aldrich, R.J. Nemanich, and D.E. Sayers, Phys. Rev. B **50**, 15 026 (1994).
[12] J.C. Aubry, T. Tyliszczak, A.P. Hitchcock, J.M. Baribeau, and T.E. Jackman, Phys. Rev. B **59**, 12 872 (1999).
[13] M.C. Ridgway, K.M. Yu, C.J. Glover, G.J. Floran, C. Clerc, J.L. Hansen, and A. Nylandsted Larsen, Phys. Rev. B **60**, 10 831 (1999).
[14] Y. Kuwahara, H. Oyanagi, R. Shioda, Y. Takeda, H. Yamaguchi, and M. Aono, Jpn. J. Appl. Phys., Part 1 **33**, 5631 (1994).
[15] M. Tabuchi, T. Kumamoto, and Y. Takeda, J. Appl. Phys. **77**, 143 (1995).
[16] J.C. Woicik, J.G. Pellegrino, B. Steiner, K.E. Miyano, S.B. Bonpadre, L.B. Sorensen, T.-L. Lee, and S. Khalid, Phys. Rev. Lett. **79**, 5027 (1997).
[17] F. Romanato, D. De Salvador, M. Berti, A. Drigo, M. Natali, M. Tormen, G. Rossetto, S. Pascarelli, F. Boscherini, C. Lamberti, and S. Mobilio, Phys. Rev. B **57**, 14 620 (1998).
[18] M. Tormen, D. De Salvador, M. Natali, A. Drigo, F. Romanato, G. Rossetto, F. Boscherini, and S. Mobilio, J. Appl. Phys. **86**, 2533 (1999).
[19] S. Pascarelli, F. Boscherini, F. D'Acapito, J. Hrdy, C. Meneghini, and S. Mobilio, J. Synchrotron Radiat. **3**, 147 (1996).
[20] M. Tormen, D. De Salvador, A. Drigo, F. Romanato, F. Boscherini, and S. Mobilio (unpublished).
[21] J. Tersoff, Phys. Rev. B **39**, 5566 (1989).
[22] P.C. Kelires, Int. J. Mod. Phys. C **9**, 357 (1998).
[23] M. Berti, D. De Salvador, A.V. Drigo, F. Romanato, J. Stangl, S. Zerlauth, F. Schäffler, and G. Bauer, Appl. Phys. Lett. **72**, 1602 (1998).
[24] D. Mura, L. Colombo, R. Bertoncini, and G. Mula, Phys. Rev. B **58**, 10 357 (1998).
[25] M. Berti, D. De Salvador, A.V. Drigo, F. Romanato, A. Sambo, S. Zerlauth, J. Stangl, F. Schäffler, and G. Bauer, Nucl. Instrum. Methods Phys. Res. B **143**, 357 (1998).
[26] J.F. Ziegler, *Stopping Power and Ranges of Ions in Matter*, Vol. 4 (Pergamon Press, New York, 1997).
[27] D.C. Santry and R.D. Weiner, Nucl. Instrum. Methods **178**, 523 (1978).
[28] M. Tormen, D. De Salvador, M. Natali, A.V. Drigo, F. Romanato, G. Rossetto, F. Boscherini, and S. Mobilio, J. Appl. Phys. **86**, 2533 (1999).
[29] M. Newville, P. Livins, Y. Yacoby, J.J. Rehr, and E.A. Stern, Phys. Rev. B **47**, 14 126 (1993).
[30] J. Mustre de Leon, J.J. Rehr, S.I. Zabinsky, and R.C. Albers, Phys. Rev. B **44**, 4146 (1991).
[31] M. Newville, B. Ravel, D. Haskel, J.J. Rehr, E.A. Stern, and Y. Yacoby, Physica B **208-209**, 154 (1995).
[32] Normand Mousseau and M.F. Thorpe, Phys. Rev. B **46**, 15 887 (1992).
[33] J. Tersoff, Phys. Rev. B **38**, 9902 (1988).
[34] M.P. Allen and D.J. Tildesley, *Computer Simulation of Liquids* (Oxford University Press, New York, 1990).
[35] H.C. Andersen, J. Chem. Phys. **70**, 2384 (1980).
[36] F. Boscherin, C. Lamberti, S. Sakura, A. Rigo, and S. Mobilio, Phys. Rev. B **58**, 10 754 (1998).